ELSEVIER

Contents lists available at ScienceDirect

# Acta Materialia

journal homepage: www.elsevier.com/locate/actamat



# Full length article

# Concurrent prediction of metallic glasses' global energy and internal structural heterogeneity by interpretable machine learning

Chaoyi Liu  $^{a,1}$ , Yuchu Wang  $^{a,1}$ , Yuchi Wang  $^b$ , Minhazul Islam  $^b$ , Jinwoo Hwang  $^b$ , Yunzhi Wang  $^b$ , Yue Fan  $^{a,*}$ 

# ARTICLE INFO

# Keywords: Metallic glasses Machine learning Structure-property relationship Heterogeneity

#### ABSTRACT

Predicting glasses' properties from their structures is a formidable challenge because of the inherently disordered atomic configurations. Here we tackle the problem using a new two-stage (encoding/interpreting) machine learning pipeline. First, local environments are encoded by the Smooth Overlap of Atomic Positions (SOAP) descriptors, which are then fed into extreme gradient boosting tree algorithm to train/predict given samples' configurational energy. 40 important unique local environments (ULEs) most responsible for the global energy of ZrCu-based glasses are identified. Markedly, we discover that the same short-range orders of Voronoi cells, when embedded in various ULEs, could impact the sample's global stability in qualitatively different manners. These new findings thus reveal a profound connection between short-range orders and medium-range orders. In the second stage, a designed interpreting stage is employed to decompose a sample's 3 N degrees-of-freedom configuration into a 40-dimension probability spectrum barcode via frequency mapping of those ULEs. We demonstrate that, in addition to the global energy prediction, by analyzing barcode-elements' occupational fractions and fluctuations, one can simultaneously assess samples' structural heterogeneity, which is known as a crucial quantity to dictate metallic glasses' deformation behaviors. The implications of our findings to a barcode-mediated new strategy of inverse engineering design of metallic glasses are also discussed.

# 1. Introduction

Amorphous solids such as metallic glasses exhibit unique performance in many aspects of physical and mechanical properties, ranging from load bearing [1,2] to energy dissipation [3,4], thermal stability [5], corrosion, and damage resistance [6,7], and magnetism and electronics [8]. From the cornerstone perspective of the entire materials science, namely the "structure-property" relationship, all those properties mentioned above should be ultimately entailed in the configurations of constituent particles inside the materials. However, albeit the fact that glasses and crystals share many similar mechanical behaviors [9–14], building an effective structure-property relationship in glasses has been far less successful than that in their crystalline counterparts, mainly due to the complex duality nature of atomic packing in amorphous solids – globally random and meanwhile internally non-uniform (as manifested by the non-affine and heterogeneous local strain partitions upon loading). In other words, a robust description of glassy materials has to

satisfy two stringent requirements: On the one hand, it ought to extract key global features (*e.g.*, enthalpy, fictive temperature, or other indicators) that are known to dictate macroscopic properties [15–17] (*e.g.*, bulk modulus, ductility); On the other hand, it ought to include various local structural features (*e.g.*, packings/configurations of atom clusters) that account for mechanical and dynamical heterogeneities [18–22] (*e.g.*, spatial sensitive energy dissipation and  $\beta$  relaxations). Among a plethora of efforts, probably one of the most influential models is the Voronoi tessellation-based short-range orders (SROs) analysis [23], where distributions of various types of SROs define the materials' properties, *e.g.*, the statistical correlation between the fraction of high-symmetry SROs (*i.e.*, icosahedron) in a given system and its overall stability [24–26]. Despite its great success, a more quantitative relation is still lacking, due to the diversity of SROs and the subtle differences between similar Voronoi cells [27].

Machine learning (ML) algorithms, as emerging powerful techniques, have recently been utilized to probe and predict a variety of

a Department of Mechanical Engineering, University of Michigan, Ann Arbor, MI, United States

<sup>&</sup>lt;sup>b</sup> Department of Materials Sciences and Engineering, Ohio State University, Columbus, OH, United States

 $<sup>^{\</sup>star}$  Corresponding author.

E-mail address: fanyue@umich.edu (Y. Fan).

<sup>&</sup>lt;sup>1</sup> These authors contributed equally to this work.

properties in amorphous solids, from system-level properties such as glass formability [28] and elastic moduli [29], to regional behaviors such as the softness [30,31] and responsiveness of local atomic configurations upon excitation [27], and to the force field development between atom pairs [32]. Despite tremendous progress, the duality requirement posed above has not been well addressed. In addition, many existing ML models are more or less black boxes in nature, causing a compromised interpretability and limited extendibility. In other words, the critical questions as to what physical insights one can learn from the data-driven techniques, how they are connected to, and how they can further advance people's existing knowledge in the field, remain as demanding challenges.

To resolve the issues identified above, in the present study, we report a new ML pipeline, in which two key strategies are adopted. At first, instead of using scenario-specific supervisory signals (e.g., hopping rates or non-affine displacements under a particular loading condition), we use the most fundamental and accessible information – particles' static spatial coordinates - as the baseline input for encoding. With such deliberation, we can avoid the model being "trained on one specific behavior, tested and meant for recognizing that particular behavior for the most part" [27], so that its extendibility can be improved. Secondly, while the model is trained with a local structural basis, we design an interpreting stage (Fig. 1) to represent the global structure in terms of the spectrum distribution of those learned important local environments. This serves as a bridge to comprehend the data and correlate them with existing knowledge (e.g., SROs and medium-range orders as discussed below), which enables better interpretability of our model. Tested with a widely used ZrCu-based metallic glass model [24], we show that the hereby proposed encoding-interpreting pipeline can boil down the 3D configuration of a given sample into a spectrum barcode spanned by 40 most important unique local environments (ULE) extracted from ML algorithm based on their contribution scores in the training process. The so-learned 40 indices can be classified into two categories according to the symmetries of their ULEs. We further demonstrate that, the relative occupational fraction of each category

determines the sample's global stability/energy, while the fluctuations of the indices inside the low-symmetry-ULEs category dictate the sample's intrinsic structural heterogeneity. These findings mark a new way to decipher disordered materials, which, in further conjunction with inverse problem solvers (e.g., reverse Monte Carlo method), may enable a strategy to build up an amorphous solid's configuration with desired global and local properties, simultaneously.

# 2. Materials and methods

#### 2.1. Samples preparation

Our first-step goal is to reliably predict a metallic glass sample's global stability/energy with arbitrary input configuration. Here we use inherent structure (IS) energy as an effective measure of the sample's global stability because of both its easiness in computing and its proven robustness in measuring glassy materials' many important global properties [33–39]. A cooling–annealing protocol is applied in this study to prepare sufficient samples at various IS configurations and energy levels. To be more specific, samples are firstly equilibrated in liquid states at 2000 K and then quenched down to 0 K with controlled cooling rates, which vary from  $10^{13}$  to  $10^{10}$  K/s. To prepare more stable configurations, some of the above samples are elevated to and held for 10 ns at a temperature window (500  $K \sim 700 K$ ) close to the glass transition temperature ( $T_g \sim 700 \text{ K}$  for the present model [40]). Because it is known that the near- $T_g$  annealing treatment can significantly stabilize the glassy systems, leading to equivalently very low cooling rates comparable with real experiments [41,42]. This way, a multiplicity of different inherent structures is produced spanning over a wide range of energy levels, and altogether we have collected 10,000 different Zr<sub>44</sub>Cu<sub>56</sub> glass samples (2000 atoms in each sample). These samples' IS energies are then served as the training and testing supervisory signals in the present study. We would like to note that there is room for annealing protocol optimization [42,43] or even different algorithm [37,44] that can further stabilize the glass samples. Nevertheless, given that our main

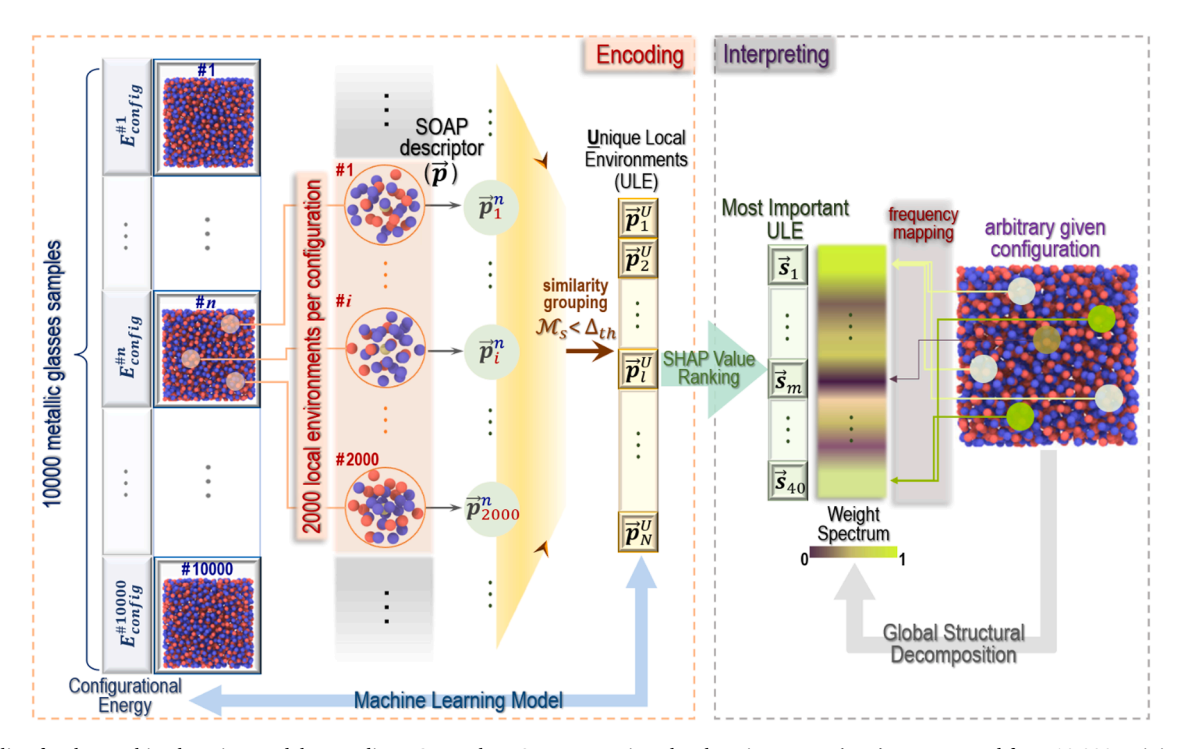


**Fig. 1.** Pipeline for the machine learning model to predict MG samples' IS energy. Unique local environments (ULE) are extracted from 10,000 training samples by scanning all the local environments and picking the representative cluster by a proper similarity threshold. By further comparing the ULEs' SHAP contribution scores in ML, 40 most important ULEs are extracted. Then in the interpreting stage, a given sample's 3D configuration with 3 N degrees of freedom is boiled down to a 40-dimensional probability vector, in which each entry represents the fraction of the corresponding ULE in the sample.

purpose here is not to produce the most stable configuration but instead to efficiently generate large amount of samples covering broad energy space (and subsequently a wide variety of ULEs), the hereby adopted protocol can therefore well serve the purpose.

As discussed earlier, to improve the interpretability and extendibility

# 2.2. ML framework

of this work, we adopt an encoding-interpreting pipeline illustrated in Fig. 1. The atomic structures are examined and encoded by the Smooth Overlap of Atomic Positions (SOAP) descriptor [45,46], which essentially expands the Gaussian density distributions of a local cluster of particles into spherical harmonics power spectrum (e.g.,  $\overrightarrow{p}$  vector illustrated in the encoding panel of Fig. 1). As a compactly supported function, the SOAP descriptor goes smoothly to zero and can be expanded to an arbitrary desired accuracy. In addition, with its proven stability against the operations such as translation, rotation, permutation, and deformation, the SOAP descriptor has been widely applied in disordered structural environments [47–50]. More specifically, we take the cut-off radius of SOAP descriptors  $r_{cut}$  as 5.0 Å, the number of radial basis functions  $n_{max}$  as 11, the maximum degree of spherical harmonics  $l_{max}$  as 12, and the standard deviation of the gaussians used to expand the atomic density  $\sigma$  as 0.5. We apply the DScribe package to do the calculations, where periodic boundary conditions are considered. Since each individual sample in the present study allows an extraction of 2000 local environments, the total number of local environments across all the prepared samples would be enormous. As illustrated in the left panel of Fig. 1, here we compare the similarities of those raw power spectra and group them into a number of unique local environments (ULEs). More specifically, the similarity is measured as  $M_s = 1$  $\sqrt{(\overrightarrow{p}_i - \overrightarrow{p}_i)^2}/2$ , and two local environments are regarded as ULEs only if they exhibit a low level of similarity smaller than a threshold  $\Delta_{th}$ . This similarity threshold is critical because in disordered systems, no two local environments would be entirely identical, and each local environment after the SOAP encoding would in principle be different from others. Therefore, with a threshold screening, one can effectively reduce the dimension of the learning space and avoid the issues like overfitting, allowing physical and interpretable insights to be better extracted from the model. The final dimension of ULEs is of course dependent on the selection of threshold value, and in the present study we find that 5223 ULEs are extracted with  $\Delta_{th} = 0.84$ . Once the 5223 ULEs are identified, the glassy structures can be encoded by calculating the corresponding ULEs fractions using the same threshold of  $\Delta_{th} = 0.84$ . For each atom in a sample, one can find the ULEs having the highest similarities with the atom's SOAP descriptor. Then, the entry at the corresponding position in the 5223-dimensional vector would be registered. After scanning all the atoms in the given sample, an associated signature vector in the space spanned by the ULEs would be generated. In sum, from the 10,000 samples, we can get a feature matrix with the dimension of 10,000  $\times$ 5223, and the dimension of the label vector would be  $10,000 \times 1$ , which is the real total energy of the samples. We have also found that using the 5223 ULEs to establish the datasets can already control the errors of IS energy predictions less than  $5.0 \times 10^{-4}$  eV/atom. Note that there is plenty of room for further ML parameters optimization and error reduction (Fig. A1 in Appendix). While here in the main text, our primary goal is not to pursue the highest numerical precision but instead to

# 2.3. Training model and parameters

With the hereby obtained ULEs, the next important step is to pick a proper ML model to learn from them and eventually predict a given sample's IS energy. There are a wide variety of ML algorithms that have

unveil the physical insights from an interpretable ML framework.

Therefore, the following discussions are based on the same volume of

training dataset and the same similarity threshold value.

been applied to study amorphous materials, including logistic regression [51], support vector machine (SVM) [52,53], neural network [54], gradient boosted trees [55], etc. Here we employ extreme gradient boosting tree (XGBoost) [56] - an algorithm under the gradient boosted trees family - as our ML model because it is computationally efficient and meanwhile also offers a high level of transparency compared with other models such as neural network. The parameters of XGBoost are determined by the Bayesian optimization process. We use the 5-fold validation procedure, and the explored parameter space is set as: (20, 40) for max\_depth, (0.01, 0.05) for eta, (0.001, 10.0) for gamma, (0, 2000) for min\_child\_weight, (0.4, 1.0) for subsample, (0.4, 1.0) for colsample\_bytree. The parameter of the early stopping rounds is set to 100. With the help of Bayesian optimization, the best machine learning model is trained from {max\_depth, eta, gamma, min\_child\_weight, subsample,  $colsample\ bytre\} = \{20,\ 0.0271589,\ 0.01878,\ 82.011109,\ 0.767066,\ 0.018780,\ 0.018780,\ 0.018780,\ 0.018780,\ 0.018780,\ 0.018780,\ 0.01878$ 0.623959}. Python xgb library is used for training, feature selection and model iteration.

To further improve the interpretability of our present study, the ULEs used in the encoding stage are ranked according to their SHapley Additive exPlanations (SHAP) [57,58] values, which give quantitative measures on their relative feature importance. It is found that, according to the SHAP scores distributions for all 5223 ULEs (Fig. A2 in Appendix), there are about 40 ULEs showing relatively higher significance than others. We hence regard them as the most important ULEs as our final representation bases for the metallic glasses considered in this work. Then it comes to the interpreting stage illustrated in the right panel of Fig. 1, where a given sample is decomposed into a 40-dimension probability vector via frequency mapping of its local environments, denoted as  $(s_1, s_2, \dots, s_{40})$ .

#### 3. Results

# 3.1. Global energy prediction

Fig. 2 exemplifies a few cases of probability spectrum barcode representation for different samples, and the overall energy prediction performance of our ML model on the independent testing datasets is also shown on the left. More specifically, after the training with the 2000atoms samples dataset discussed above, we generate another 10,000 testing samples for the 2000-atoms system, which have been prepared independently and not involved in any stage of the training process. It can be seen that even within such largely reduced 40-dimension space the accuracy of energy prediction retains at a high level, with the root mean square error (RMSE) of 2.3624 eV per system (i.e., error around  $10^{-3}$  eV/atom). It is also worth marking that since through the designed interpreting stage any input sample is boiled down to a probability representation, there is therefore no size limitation in our model. To demonstrate this, in the inset of Fig. 2 we present the direct testing results on 2000 new testing samples for a larger 4000-atoms system without any new training, and the predictions are aligned well with the diagonal line. The error distributions follow a typical Gaussian profile and are found independent of the sizes of testing samples (Fig. A3 in Appendix). In other words, the hereby learned ULEs already capture almost all the crucial structural information in metallic glasses, at least in the Zr<sub>44</sub>Cu<sub>56</sub> model considered in the present study. As discussed in Supplemental Materials, although our present study was only trained in the Zr<sub>44</sub>Cu<sub>56</sub> system, it still offers certain flexibility in predicting other compositions without new training. Such flexibility comes from the variety of ULEs extracted by our ML model because each ULE has its own local composition (as seen in Fig. 3). For materials with very different chemistries or compositions, the specific ULEs in Fig. 3 could be different. But the methodology developed in Fig. 1 is general, and the soderived probability spectrum barcode interpretation would be broadly applicable.

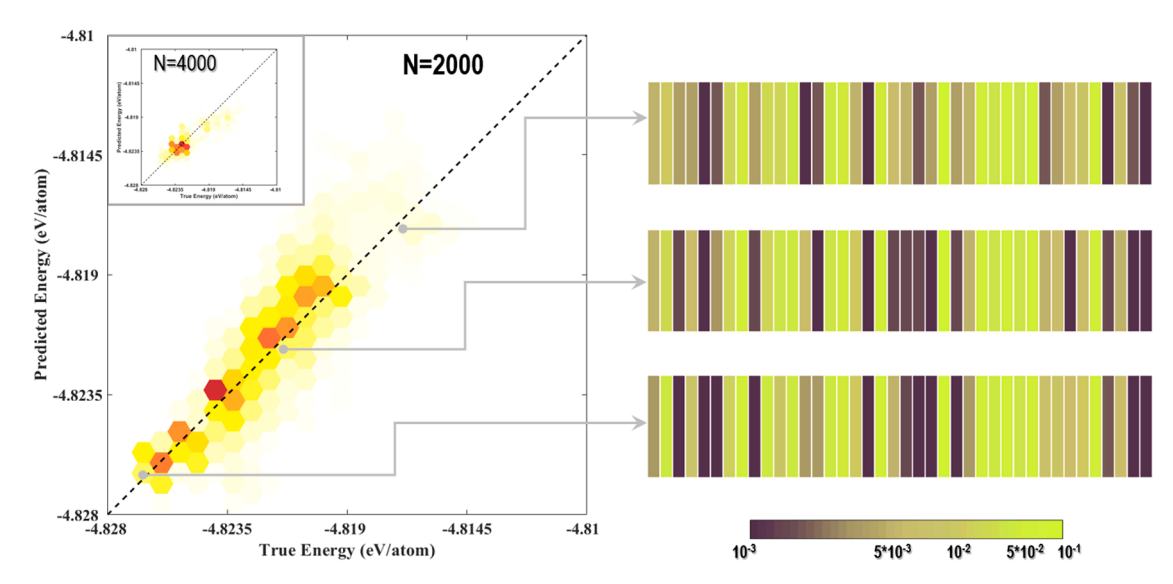


Fig. 2. Main plot on the left: ML prediction on the IS energy of 2000-atoms samples. A few representative ULE probability barcodes are listed in the right panel. The inset plot shows the prediction results of 4000-atoms samples purely based on the training in 2000-atoms samples, demonstrating the extendibility of the present ML model.

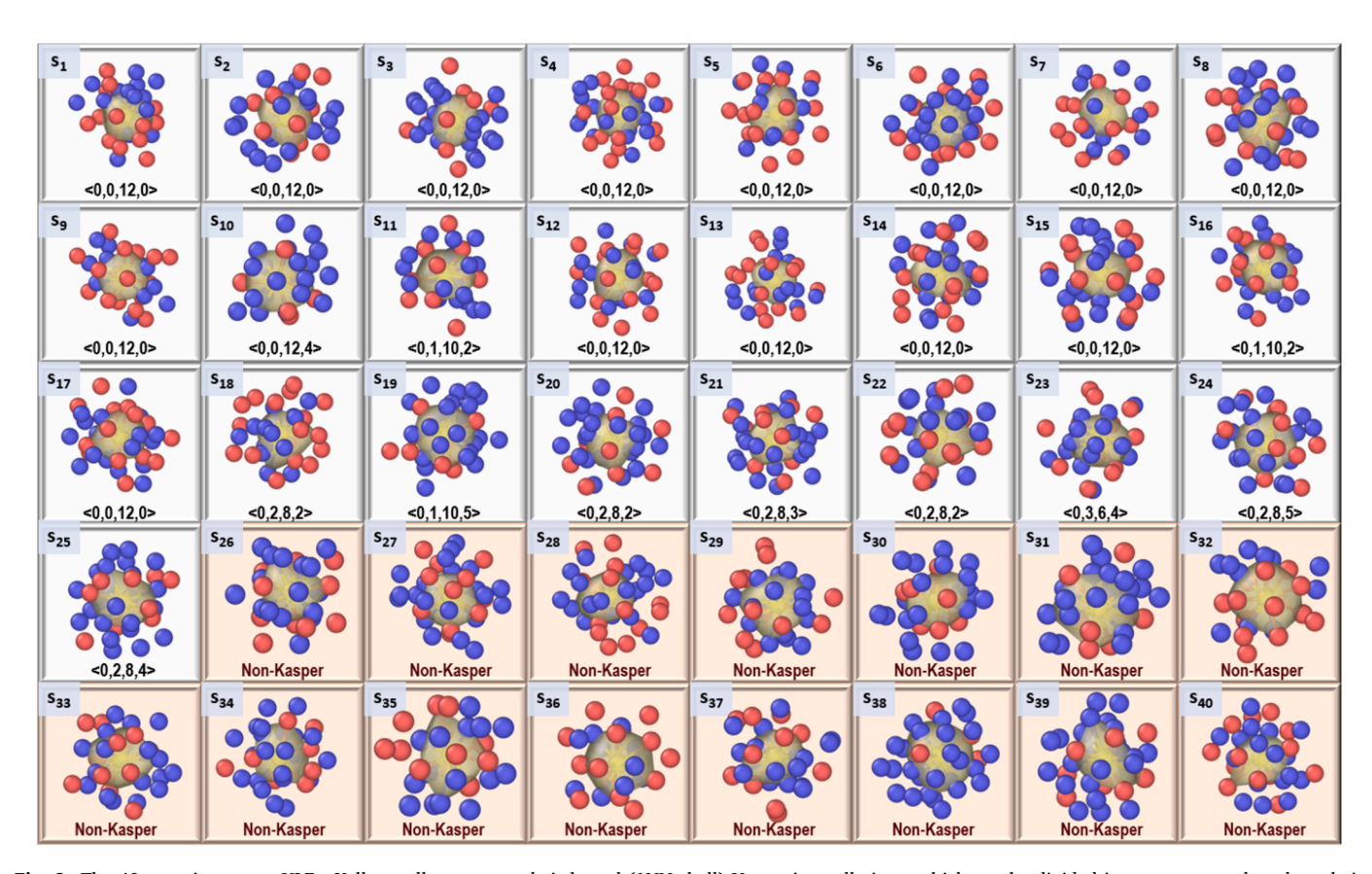


Fig. 3. The 40 most important ULEs. Yellow cells represent their kernel (1NN shell) Voronoi tessellations, which can be divided into two groups based on their Voronoi cells symmetries – the Kasper kernel  $(s_1-s_{25})$  and non-Kasper kernel  $(s_2-s_{40})$ , respectively. The SHAP value of various ULEs is shown in Appendix, Fig. A2.

# 3.2. ULEs structures and their connections to short/medium range orders

To dive deeper into the physical meaning of those ULEs and to tie them to people's existing knowledge in the field, we conduct short-range orders (SROs) analyses via 1st-nearest-neighbor (1NN) Voronoi tessellation with respect to the center atoms of interested ULEs. We would like to note, though, that the ULEs are spatially more extended than 1NN

shell. The first observation, as illustrated in Fig. 3, is that they can be divided into 2 groups. More specifically, 25 ULEs possess relatively high symmetries of their kernel SROs (i.e., indices satisfying  $2n_4+n_5=12$ ), while in the rest 15 ULEs their kernel SROs are non-Kasper clusters. Given the comparable sizes of the two groups (25 vs. 15), it indicates that both symmetric and asymmetric SROs are important in determining the properties of metallic glasses. This corroborates well with the picture

established in previous studies [18,25,59], namely the mutual importance of icosahedra and geometrically unfavorable motifs. It is worth emphasizing that we have not provided any SROs information *a priori*, and these important ULEs are automatically extracted purely based on the static configurations of input training samples. In other words, the consistencies with earlier studies manifest the effectiveness of our ML model

Another critical observation is that SROs information alone cannot sufficiently well describe metallic glasses. More specifically, as shown in Fig. 3, there are multiple different ULEs sharing the same index of their kernel SROs. This equivalently means that the same SROs do not necessarily yield the same properties, and they may lead to different impacts on the samples' global energy when being embedded in various ULEs. For example, it has been widely believed that icosahedra (i.e., (0,0,12,0) Voronoi index) in metallic glasses have a propensity for stability [25], a scrutiny of the Pearson correlation coefficients between each individual ULEs and the samples' global energy shown in Fig. 4, however, suggests a diverse result. More specifically, while some icosahedra-containing ULEs (e.g., s2, s8, s15, etc.) exhibit an as-expected negative correlation with system's global energy, some other icosahedra-containing ULEs (e.g., s<sub>1</sub>, s<sub>3</sub>, s<sub>5</sub>, etc.) actually show an inverse correlation. This indicates that a higher fraction of icosahedra does not necessarily always lead to a more stable metallic glass sample. Such new knowledge is beyond what the conventional Voronoi cells-based SROs statistics can provide, and it, therefore, sheds more in-depth insights into the understanding of metallic glasses. Note that there is an increasing consensus among the community that medium-range orders (MROs) must play an indispensable role in amorphous materials [59-63], and our present study lends credence to such a notion. Furthermore, while it is beyond the scope the present study, it is worth marking that the combined XGBoost and SHAP ranking algorithms allow one to quantitatively measure and compare the relative importance of various ULEs, which may thus enable a quantitative analysis on the SROs-MROs connections that warrant future studies.

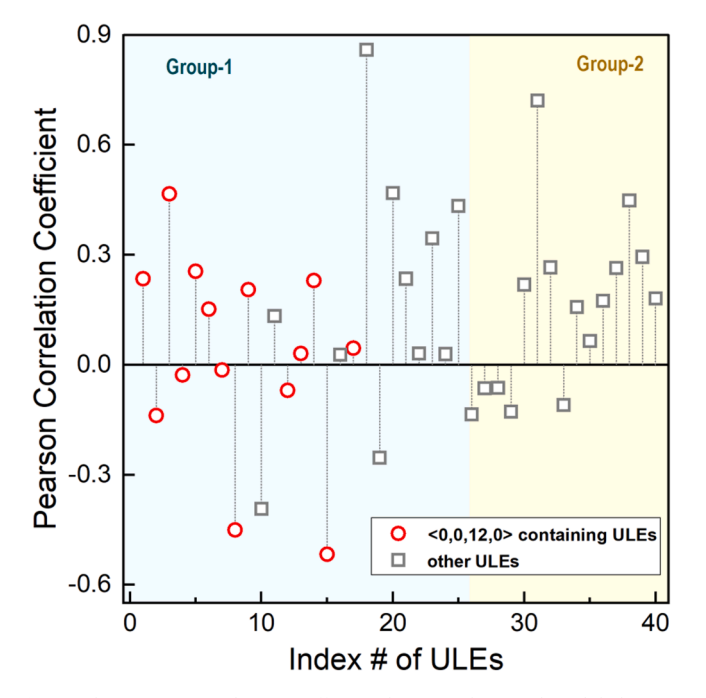


Fig. 4. The Pearson correlation coefficients between the samples' global energy and each of the 40 most important ULEs. The ULEs containing  $\langle 0,0,12,0\rangle$  SRO kernels are marked with red circles, while others are represented by gray squares.

#### 3.3. Structural heterogeneity entailed in the spectrum barcode

In addition to the global stability, a glass sample's intrinsic structural heterogeneity – e.g., non-uniform partitions of strains across the sample upon loading - plays a decisive role in its deformation behavior [19-22, 64,65]. We demonstrate in this section that such heterogeneity information is to some extent entailed in the 40-dimensional probability spectrum barcode generated by our ML model. To begin with, we prepare and contrast the samples with different levels of structural heterogeneities. The relatively less heterogeneous samples are prepared via thermal processing, during which a controlled cooling treatment is uniformly introduced into a high-temperature equilibrated supercooled liquid. As discussed in Section 2.1 and illustrated in the left panel of Fig. 5, by tuning the annealing time a multiplicity of samples across a broad IS energy range can be generated. The structurally more heterogeneous samples are prepared via various thermo-mechanical loadings shown in the right panel of Fig. 5. More specifically, Lees-Edwards boundary conditions are used to impose the global shear deformation at a controlled strain rate of  $10^7$  s<sup>-1</sup>. The operational temperatures vary from 300 K to 700 K, and lower temperature leads to more heterogenous structures. The sample can thus be driven to various steady-state flow states with distinct energies and heterogeneities, as illustrated in the right panel of Fig. 5. We would like to emphasize that the mechanical loading condition applied here is a typical MD strain rate that is much higher than normal mechanical testing in experiments. However, it is worth noting that the purpose of the MD simulations here in the right panel of Fig. 5 is not to retrieve the mechanical properties such as yield strength at various thermo-mechanical conditions. Instead, the purpose is to utilize mechanical loading as a knob to drive the samples to heterogeneous structures (e.g., with shear banding inside), so that one can compare with those more homogenous thermally processed samples and examine whether or not our ML model can capture the structural heterogeneity information.

We show a few examples in the figure on the atomic-level von Mises strain distributions in differently prepared samples, and one can confirm that the mechanically driven structures are in general more heterogeneous, while the level of heterogeneity increases as temperature decreases. In other words, as illustrated in Fig. 5, by comparing the thermally processed and mechanically driven samples at the same energy levels one can then probe how the structural heterogeneity information would be reflected in the spectrum barcode.

A systematic comparison is shown in Fig. 6, where two remarkable features are revealed. At first, as long as the energy levels are consistent, the thermally processed samples and the mechanically driven samples always present similar values of  $\sum_{1}^{25} s_i$  (or  $\sum_{26}^{40} s_i$ ), although a clear quantitative correlation remains unclear (see Fig. 7 in Discussion section below for more discussion). Secondly, by scrutinizing the differences between the spectrum barcodes, denoted as  $\delta \vec{s} \equiv \vec{s}_{th} - \vec{s}_{mech}$ , it is discovered that the standard deviation of  $\delta s_i$  in Group-2 exhibits a strong correlation with the heterogeneity level. In particular, the more heterogeneous the samples are (e.g., M300), the larger the standard deviations of the data entries  $[\delta s_{26}, \dots, \delta s_{40}]$  one can expect. By contrast, the standard deviation of  $\delta s_i$  in Group-1 is almost flat and not sensitive to a sample's heterogeneity level. It is worth noting that, all the training and learning in the present study are based on thermally processed samples only. And the fact this model can grasp information on the structural heterogeneity level of a deformed sample is unexpected and profound. It demonstrates the hereby obtained important ULEs, as well as their probability spectrum representations, are effective ways to decipher amorphous solids in general thermo-mechanical environments.

# 4. Discussion

In the present work a new ML pipeline is developed to study the structures and properties of amorphous solids. We employ the SOAP

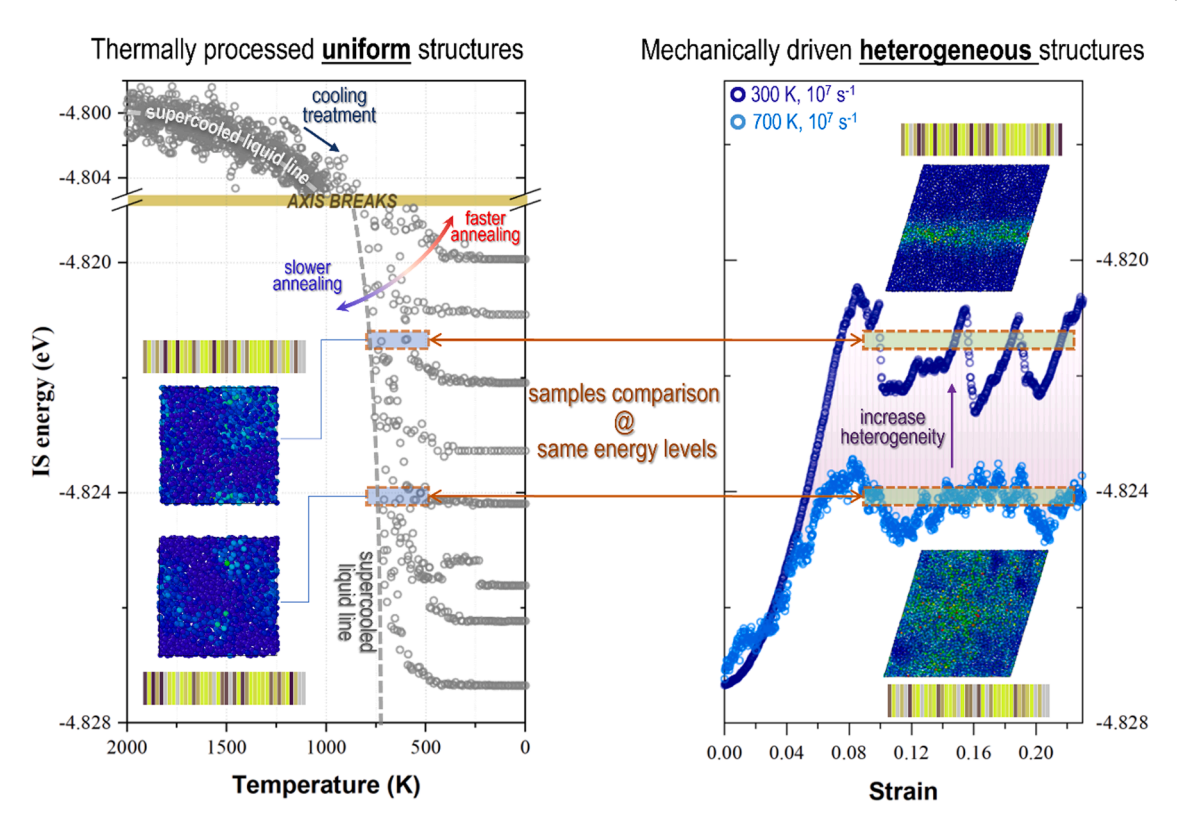


**Fig. 5.** (Left) Preparing samples with relatively uniform structures at various energy levels by controlling annealing protocols. (Right) Preparing samples with heterogeneous strain distributions by mechanically driving at different temperatures. By comparing the barcodes of the samples at the same energy levels between the left and right panels, one can then probe how the structural heterogeneities are entailed in the barcodes. Note that there were no new trainings for the shear-loaded samples. In other words, their barcodes are generated using the same ML model based on the trainings only on thermally processed samples, as explained above in Fig. 1. It is also worth noting that, the mechanical loading condition applied here is a typical MD strain rate that is much higher than normal mechanical testing in experiments. However, the purpose of the simulations in the right panel is not to retrieve the mechanical properties such as yield strength at various thermo-mechanical conditions. Instead, the purpose is to utilize mechanical loading as a knob to drive the samples to heterogeneous structures (e.g., with shear banding inside), so that one can then compare with those more homogenous thermally processed samples and examine whether the present ML model can capture the structural heterogeneity information.

descriptor to encode the local environments, which are then fed into the extreme gradient boosting tree algorithm to train, learn, and eventually predict the global configurational energy of metallic glasses. By comparing the SHAP scores of various local environments, we identify 40 important ULEs that are most responsible for the IS energy of a given glass sample. A designed interpreting stage is then employed to decompose a given sample's 3 N degrees of freedom configuration into a 40-dimension probability vector via frequency mapping of those ULEs. The obtained probability spectrum barcode is thus regarded as a signature representation of an interested sample. We demonstrate that the so-constructed encoding-interpreting pipeline can reliably predict metallic glasses samples' energy within the error of  $10^{-3}$  eV/atom. It is worth noting that, with the hereby constructed probability spectrum representation there is no size constraint to this model. We demonstrate that the important ULEs learned/extracted from smaller samples can be readily used to predict the energy of larger samples without the necessity of any new trainings, which marks an enhanced extendibility of the present study. Note that if a new configuration has none of those 40 ULEs then technically its probability vector would be zero. This would mean the input sample is completely out of the scope of our present study (e.g., at non-glassy state or fundamentally different chemistry/ composition). But such a scenario is not likely to occur for the ZrCu metallic glasses concerned in our present study. Because as discussed above, the simulation samples we used to train the model actually cover a broad range of effective cooling rates, including conditions comparable with real experiments. Therefore, it is likely that all the important ULEs in the ZrCu system are already captured by our ML model. This is also supported by the fact that our model can reasonably well predict larger samples' global energy without any new training.

Further topological analyses to the kernel structures (e.g., within 1NN shell) of ULEs reveal two notable findings. At first, both symmetric SROs (Group-1) and geometrically unfavored motifs (Group-2) are important. This is markable not only because they are consistent with people's knowledge in the field through a number of earlier studies, but also because we have not provided any SROs information a priori, and the important ULEs are automatically extracted solely based on particles' static spatial coordinates. Secondly, it is discovered that different ULEs may share the same kernels of SROs. This suggests the insufficiency of SROs in quantitatively describing amorphous solids and thus lends further credence to the increasing appreciation of MROs by the community in recent years. More specifically, the ULEs-based probability spectrum barcode constructed in the present study may offer a viable pathway moving forward to help people better connect SROs and MROs. For example, as discussed earlier, by using XGBoost and SHAP algorithms the relative importance of each entry in the ULEs spectrum barcode can be quantitatively measured. This eventually will allow one to answer critical questions such as, how a specific SRO, when embedded into various MROs, would differently impact the sample's property. This will be discussed in a separate study in the future.

It is noteworthy that, in addition to the high-fidelity prediction of global energy, a sample's signature probability spectrum barcode also entails important information on its intrinsic structural heterogeneity. To better understand this, one can first set the thermally prepared samples and their corresponding barcodes (e.g., the ones with "Thermal" label in Fig. 6) as the references for the following considerations: (a) Thermal processing is arguably the most widely used simple protocol in

C. Liu et al. Acta Materialia 259 (2023) 119281

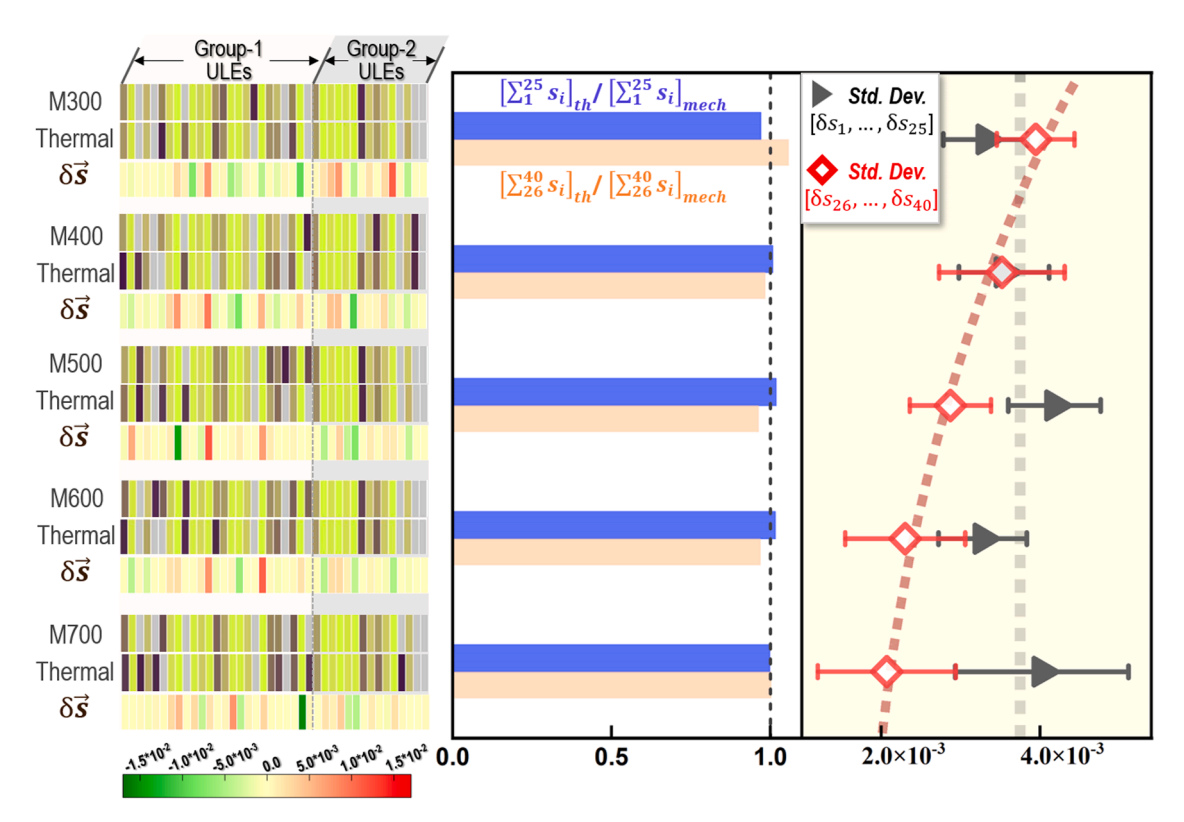


**Fig. 6.** (Left) Barcodes comparisons for the thermally prepared samples and mechanically driven samples at the same energy levels. (Middle) The corresponding ratios of Group-1 entries  $\sum_{1}^{25} s_i$  (blue bars) and Group-2 entries  $\sum_{26}^{40} s_i$  (orange bars) between the thermally prepared samples and mechanically driven samples are always close to 1. (Right) The standard deviations of the barcodes contrast vectors  $\delta \vec{s}$ , as well as the associated error bars, in particular, the data entries in Group-2 [ $\delta s_{26}, \dots, \delta s_{40}$ ], exhibit a strong correlation with samples' strain heterogeneities (red dashed curve).

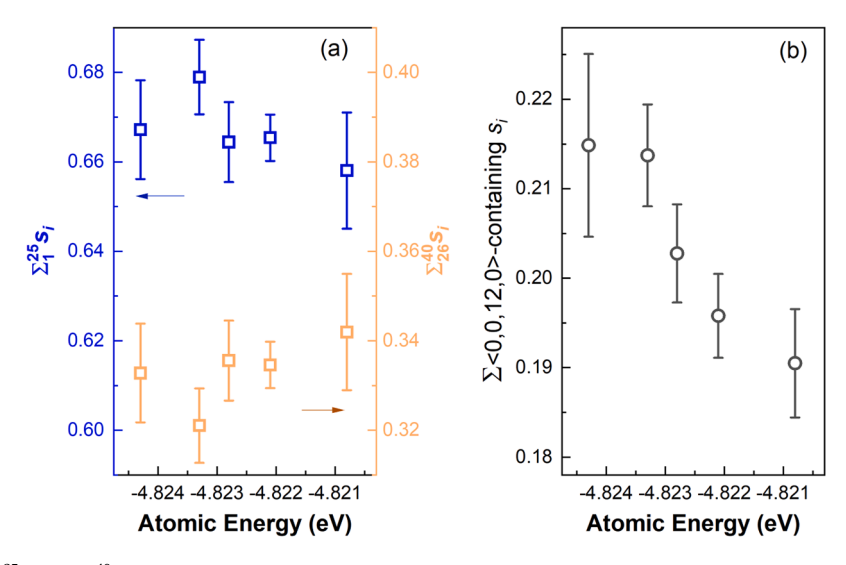


Fig. 7. (a) Relation between  $\sum_{i=1}^{25} s_i$  and  $\sum_{i=1}^{40} s_i$  with the system's global energy. (b) Relation between the summation of those <0,0,12,0>-containing ULEs and the system's global energy.

both experiments and atomistic modeling to prepare metallic glasses with good reproducibility, making them a natural choice for reference states; (b) In a statistical sense, thermally processed metallic glasses samples are known isotropic or do not exhibit system-level heterogeneities, making them a good choice to better contrast the structural heterogeneity in mechanically driven samples. Now with these clearly defined reference states, one can then better interpret the heterogeneity levels of mechanically driven samples from their barcodes. As shown in Fig. 6, through systematic comparisons between the thermally processed

references and the mechanically driven samples, it is found that the probability distributions and fluctuations of those ULEs in Group-2 exhibit a strong correlation with the level of structural heterogeneity. More specifically, a structurally more heterogeneous sample is expected to show a larger standard deviation over the probability difference entries  $[\delta s_{26}, \cdots, \delta s_{40}]$ .

In a nutshell, for an arbitrary given sample with unknown processing history, one can predict its energy and assess its heterogeneity level in two steps: (i) Analyze its ULEs and construct its barcode, from which one

can predict its global energy with the present ML model; (ii) Contrast its barcode to the reference barcode at the same global energy level, and particularly focus on the standard deviation of  $\delta s_i$  in Group-2. The larger the standard deviations of the data entries  $[\delta s_{26}, \dots, \delta s_{40}]$ , one should then expect the more heterogeneous the sample would be. The herebyestablished capability of simultaneously predicting a glassy sample's global energy and internal structural heterogeneity is markable, because it may endow promising implications in terms of deformation control. For example, it is known that the ductility of metallic glasses is largely affected by both the global energy of the samples [66] and their intrinsic structural heterogeneities [21,67]. In particular, the higher energy state (i.e., more rejuvenated) a sample is located at, the more likelihood it will yield a ductile behavior; meanwhile, the higher level of structural heterogeneity a sample possesses, the larger chance it will experience a small shear bands proliferation while avoiding the formation of a major catastrophic shear band, which is also beneficial for an overall ductile deformation. Therefore, in light of the present study, one may envisage a new barcode-oriented strategy to design amorphous solids. More specifically, one can start from a targeted 40-dimension probability spectrum barcode that possesses certain desired global energy and internal structural heterogeneity. Then the sample's structure can be built up from the bottom by adjusting the particles' spatial coordinates - this could be done via inverse engineering algorithms such as reverse Monte Carlo – until the barcode of the actual sample converges to the targeted barcode. Such a barcode-mediated simultaneous tuning on both global energy and internal structural heterogeneity would allow for more effective control over metallic glasses' deformation behavior.

Admittedly, there are questions that remain unanswered. For example, through the present study we demonstrate – assisted with ML models - one can reduce the 3 N degrees-of-freedom information (N represents the number of atoms) to 40-dimensional vector while retaining rather high prediction precisions. A natural following question would hence be, can one further reduce such 40-dimensional information into even lower dimensions in a more comprehensible manner? In Fig. 7-a below we show the correlation between the global energy of the samples considered in Fig. 6 and their corresponding  $\sum_{1}^{25} s_i$  and  $\sum_{26}^{40} s_i$ , namely the fractional summations of Group-1 ULEs and Group-2 ULEs, respectively. Note that the two groups of data are actually equivalent to each other (i.e., in mirror symmetry), because as a frequency barcode there is  $\sum_{i=1}^{25} s_i + \sum_{i=1}^{40} s_i = 1$  by definition. There may exist a weak descending (ascending) trend for the blue (orange) data points, but given the relatively large standard deviations we do not believe a quantitative and meaningful correlation can be drawn. This is not too much of a surprise from our eyes, because what was essentially done in Fig. 7-a is to reduce the information entailed in a 40-dimension vector to a simple scalar number and then examine its correlation with the system's global energy. And for a completely disordered material system such as metallic glass, it is highly doubtful whether or not there could exist such a simple reduction. In Fig. 7-b we made a similar plot, but only examining the summation of all the <0,0,12,0>-containing ULEs. Now a much stronger correlation appears, and the higher summation of those <0,0,12,0>-containing ULEs the lower energy level (i.e., more stable) the system shall stay at. Such a correlation well aligns with the consensus in the community, namely higher fraction of icosahedra SROs will increase metallic glasses' stability. But again, the standard deviations are still considerable, meaning that one cannot make highprecision predictions to given samples' energy purely based on such quantity. In contrast, by utilizing all the 40-dimensional information the ML model prediction can reach much higher precision with errors only around  $10^{-3}$  eV/atom. Therefore, to what extent one can further reduce the dimensions needed to decipher amorphous solids and meanwhile improve its comprehensibility remain as challenges to be tackle in the next step.

In addition, we employed an embedded atom method (EAM)-type interatomic potential for the present computational studies. Such an

EAM potential [24] – although has been calibrated with first-principle calculations and widely adopted by the community - is after all an empirical force field. It is noticed neural network (NN) based ML techniques have been applied in developing high-precision interatomic potentials in recent years [68]. For example, Andolina et al. recently optimized [32] the interatomic force field in the ZrCu system using a deep learning neural network algorithm, which resembles well with the density functional theory (DFT) results. Therefore, in the outlook for higher precision calculations on the structures and properties of metallic glasses in the future, it will be worth implementing such a force field into our hereby-developed interpretable and extendible two-stage (encoding/interpreting) ML pipeline in Fig. 1. It is also worth noting that, the ML-obtained probability spectrum barcode in the present study is essentially a frequency mapping of ULEs, and we have not directly provided the ULEs' spatial distribution information into the ML model. Therefore, from our perspective, the fact that our ML model can capture important non-local information, such as the structural heterogeneity level, is somewhat beyond expectation. This may imply a profound connection between the occurrence probabilities of various types of local atomic packings and their spatial correlations, which is probably mediated by some global invariants/constraints such as the fixed density or imposed boundary conditions. Note that some important concepts in the crystalline materials community, such as geometrically necessary dislocations (GNDs) [69], may share a similar spirit in terms of that they could also induce non-local effects and structural gradients. However, a thorough investigation into this problem would warrant future studies.

#### 5. Conclusion

The main conclusions of the present study are summarized below:

- With the designed encoding-interpreting strategy and extreme gradient boosting tree XGBoost ranking algorithm, 40 most important ULEs are extracted, which allows one to characterize an arbitrary given sample's 3 N degrees-of-freedom configuration with a 40dimension probability spectrum barcode that can make highprecision energy prediction of the entire sample (error less than 1 meV/atom).
- Without any provided SROs information a priori, the SHAP scores ranking and the analyses on the kernel topologies (e.g., within 1NN shell) of ML-extracted ULEs naturally reveal the significance of both symmetric SROs (Group-1) and geometrically unfavored motifs (Group-2).
- Same SROs, when embedded into various MROs, may impact the samples' global energy in qualitatively different manners. For example, a higher fraction of icosahedra does not necessarily always lead to a more stable metallic glass sample, in contrast to conventional wisdom.
- The internal structural heterogeneity level of a given sample can be assessed by contrasting its barcode with the reference barcode and scrutinizing the standard deviation of  $\delta s_i$  in Group-2. The larger the standard deviations of the data entries  $[\delta s_{26}, \cdots, \delta s_{40}]$ , the more heterogeneous the sample is expected to be.

#### **Declaration of Competing Interest**

The authors declare that they have no known competing financial interests or personal relationships that could have appeared to influence the work reported in this paper.

# Acknowledgements

The authors acknowledge the supports of NSF-DMR-2104724 (Yuchi W., M.I., Yunzhi W., J. H.) and NSF-DMR-2104136 (C.L., Yuchu W., Y. F.).

C. Liu et al. Acta Materialia 259 (2023) 119281

#### Supplementary materials

Supplementary material associated with this article can be found, in the online version, at doi:10.1016/j.actamat.2023.119281.

# **Appendix**

#### 1. Improvement of the accuracy of the current model:

In this study, our goal is to efficiently predict the global energy and structural heterogeneity of  $Zr_{44}Cu_{56}$  systems in a physically interpretable manner within acceptable numerical errors. The accuracy of our ML model could be enhanced and is ultimately determined by two main factors: the size and diversity of the training set and the number of features (*i.e.*, numbers of ULEs).

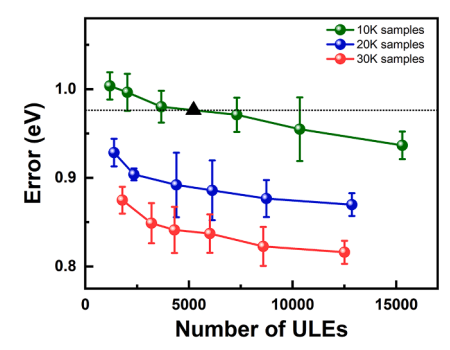


**Fig. A1.** The testing error under different ML inputs: The green, blue, and red curves have various amounts of data generated from 10, 20, and 30 independent cooling processes. The black delta point is (5223, 0.9763 *eV*), corresponding to the ML model in the manuscript of 10k samples and 5223 ULEs. Not surprisingly the training error and prediction accuracy are related to dataset volume and training algorithm [70,71].

Fig. A1 shows the prediction error of the global energy using ML models trained under different settings. From top to bottom, the three curves are models trained using different amounts of data. And each data point is an average of at least five cases. Worth noticing, for these ML practices, to explore the effect of model complexity, all the ULEs gotten from the samples are used as training features, which is different from the selection of the 40 most important ULEs in the manuscript. The black triangle and the short-dashed line depict the averaged best accuracy of the model in the manuscript, which is about 0.9763 eV for a 2000-atoms system.

The dataset is established according to the same cooling–annealing protocol depicted in the main text. The 2000-atoms samples are first equilibrated at 2000 K and then cooled to 0 K with the cooling rate range from  $10^{10}$  K/s to  $10^{13}$  K/s. Then, the energy-minimized samples are lifted to the near- $T_g$  temperature window of 500  $K \sim 700$  K and kept for 10 ns. Each cooling process would produce 1000 samples. In Fig. A1, the green, blue, and red curves have 10, 20, and 30 cooling processes, accordingly. From the curves, we can find that with a similar number of ULEs, expansion of the dataset can considerably reduce the prediction errors. In addition, for the data points on the same curve, with a fixed volume of samples, by increasing the number of ULEs (larger similarity threshold), one could also reduce the overall errors.

For the ML practices shown in Fig. A1, the smallest error we got is about 0.8159 eV for a 2000-atoms system. Technically, there is still plenty of room for improvement. However, as mentioned previously, the primary focus of this research is to build interpretable physical picture rather than pursuing the numerical precision, and such an error is acceptable.

# 2. SHAP scores distribution:

Fig. A2 below shows the SHAP values of all the 5223 ULEs retrieved in the main text under the similarity threshold of  $\Delta_{th} = 0.84$ . In the inset of Fig. A2 we show the histogram of the SHAP value distribution, and it can be seen that there is a long tail for those ULEs with SHAP value larger than 0.05, indicating their relative importance compared with others. The total number of ULEs in the long tail is around 40, and we therefore select 40 as the effective dimension to construct the probability spectrum barcode in the main body of the present study

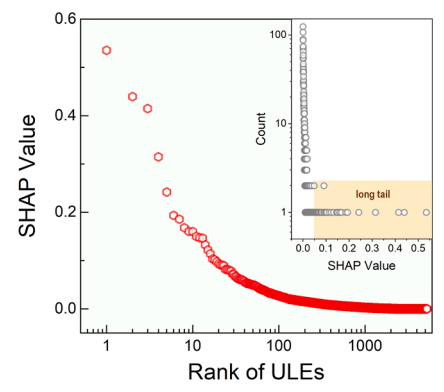


Fig. A2. The SHAP values of all ULEs. Inset plot shows the histogram of SHAP value distribution.

# 3. The distribution of testing errors:

Fig. A3 shows the probability density function (PDF) of the error distributions for both the 2000-atoms system and the larger 4000-atoms system. The blue distribution shows the error from 10,000 2000-atoms samples. The dataset of 4000-atoms samples is also prepared according to the protocol

C. Liu et al. Acta Materialia 259 (2023) 119281

in the main text. Here, 2000 samples are included in the red histogram. One can find that the two PDFs are very similar to each other, and approximately follow the Gaussian distribution.

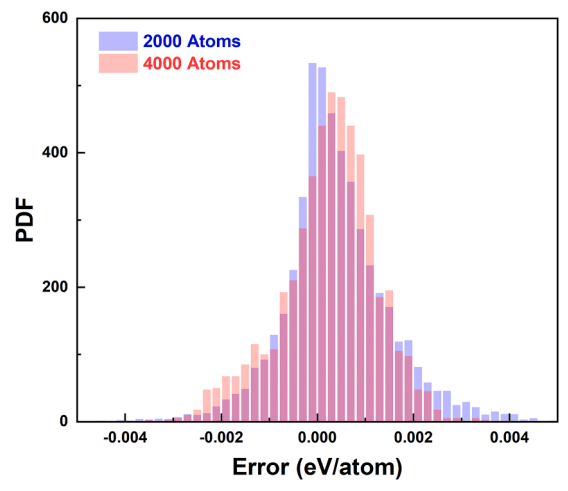


Fig. A3. The PDF of testing error for 2000-atoms samples and 4000-atoms samples. The blue histogram includes 10,000 samples while the red one includes 2000.

#### References

- [1] E.D. Cubuk, R.J.S. Ivancic, S.S. Schoenholz, D.J. Strickland, A. Basu, Z.S. Davidson, J. Fontaine, J.L. Hor, Y.R. Huang, Y. Jiang, N.C. Keim, K.D. Koshigan, J.A. Lefever, T. Liu, X.G. Ma, D.J. Magagnosc, E. Morrow, C.P. Ortiz, J.M. Rieser, A. Shavit, T. Still, Y. Xu, Y. Zhang, K.N. Nordstrom, P.E. Arratia, R.W. Carpick, D.J. Durian, Z. Fakhraai, D.J. Jerolmack, D. Lee, J. Li, R. Riggleman, K.T. Turner, A.G. Yodh, D. S. Gianola, J. Liu Andrea, Structure-property relationships from universal signatures of plasticity in disordered solids, Science 358 (6366) (2017) 1033–1037.
- [2] W.H. Wang, The elastic properties, elastic models and elastic perspectives of metallic glasses, Prog. Mater. Sci. 57 (3) (2012) 487–656.
- [3] M.M. Trexler, N.N. Thadhani, Mechanical properties of bulk metallic glasses, Prog. Mater. Sci. 55 (8) (2010) 759–839.
- [4] C. Liu, X. Yan, P. Sharma, Y. Fan, Unraveling the non-monotonic ageing of metallic glasses in the metastability-temperature space, Comput. Mater. Sci. 172 (2020), 109347.
- [5] B.W. An, E.J. Gwak, K. Kim, Y.C. Kim, J. Jang, J.Y. Kim, J.U. Park, Stretchable, transparent electrodes as wearable heaters using nanotrough networks of metallic glasses with superior mechanical properties and thermal stability, Nano Lett. 16 (1) (2016) 471–478.
- [6] M.D. Demetriou, M.E. Launey, G. Garrett, J.P. Schramm, D.C. Hofmann, W. L. Johnson, R.O. Ritchie, A damage-tolerant glass, Nat. Mater. 10 (2) (2011) 123–128.
- [7] S.J. Pang, T. Zhang, K. Asami, A. Inoue, Synthesis of Fe-Cr-Mo-C-B-P bulk metallic glasses with high corrosion resistance, Acta Mater. 50 (3) (2002) 489–497.
- [8] W. Diyatmika, J.P. Chu, B.T. Kacha, C.C. Yu, C.M. Lee, Thin film metallic glasses in optoelectronic, magnetic, and electronic applications: a recent update, Curr. Opin. Solid State Mater. Sci. 19 (2) (2015) 95–106.
- [9] H. Zhang, D.J. Srolovitz, J.F. Douglas, J.A. Warren, Grain boundaries exhibit the dynamics of glass-forming liquids, Proc. Natl. Acad. Sci. 106 (19) (2009) 7735–7740.
- [10] J. Han, V. Vitek, D.J. Srolovitz, Grain-boundary metastability and its statistical properties, Acta Mater. 104 (2016) 259–273.
- [11] T.A. Sharp, S.L. Thomas, E.D. Cubuk, S.S. Schoenholz, D.J. Srolovitz, A.J. Liu, Machine learning determination of atomic dynamics at grain boundaries, Proc. Natl. Acad. Sci. 115 (43) (2018) 10943.
- [12] Z. Bai, G.H. Balbus, D.S. Gianola, Y. Fan, Mapping the kinetic evolution of metastable grain boundaries under non-equilibrium processing, Acta Mater. 200 (2020) 328–337.
- [13] Z. Bai, A. Misra, Y. Fan, Universal Trend in the dynamic relaxations of tilted metastable grain boundaries during ultrafast thermal cycle, Mater. Res. Lett. 10 (6) (2022) 343–351.
- [14] Y. Fan, B. Yildiz, S. Yip, Analogy between glass rheology and crystal plasticity: yielding at high strain rate, Soft Matter 9 (40) (2013) 9511–9514.
- [15] L. Hornbøll, Y. Yue, Enthalpy relaxation of hyperquenched glasses and its possible link to  $\alpha$  and  $\beta$ -relaxations, J. Non-Cryst. Solids 354 (2) (2008) 350–354.
- [16] G.V. Afonin, Y.P. Mitrofanov, A.S. Makarov, N.P. Kobelev, W.H. Wang, V. A. Khonik, Universal relationship between crystallization-induced changes of the shear modulus and heat release in metallic glasses, Acta Mater. 115 (2016) 204–209.
- [17] G. Kumar, P. Neibecker, Y.H. Liu, J. Schroers, Critical fictive temperature for plasticity in metallic glasses, Nat. Commun. 4 (2013) 1536.
- [18] J. Ding, S. Patinet, M.L. Falk, Y. Cheng, E. Ma, Soft spots and their structural signature in a metallic glass, Proc. Natl. Acad. Sci. 111 (39) (2014) 14052.

- [19] F. Zhu, H.K. Nguyen, S.X. Song, D.P.B. Aji, A. Hirata, H. Wang, K. Nakajima, M. W. Chen, Intrinsic correlation between β-relaxation and spatial heterogeneity in a metallic glass, Nat. Commun. 7 (2016) 11516.
- [20] N. Wang, J. Ding, F. Yan, M. Asta, R.O. Ritchie, L. Li, Spatial correlation of elastic heterogeneity tunes the deformation behavior of metallic glasses, npj Comput. Mater. 4 (1) (2018) 19
- [21] F. Zhu, S. Song, K.M. Reddy, A. Hirata, M. Chen, Spatial heterogeneity as the structure feature for structure–property relationship of metallic glasses, Nat. Commun. 9 (1) (2018) 3965.
- [22] N. Wang, J. Ding, P. Luo, Y. Liu, L. Li, F. Yan, Chemical variation induced nanoscale spatial heterogeneity in metallic glasses, Mater. Res. Lett. 6 (12) (2018) 655–661
- [23] H.W. Sheng, W.K. Luo, F.M. Alamgir, J.M. Bai, E. Ma, Atomic packing and short-to-medium-range order in metallic glasses, Nature 439 (7075) (2006) 419–425.
- [24] Y.Q. Cheng, E. Ma, H.W. Sheng, Atomic level structure in multicomponent bulk metallic glass, Phys. Rev. Lett. 102 (24) (2009), 245501.
- [25] Y.Q. Cheng, E. Ma, Atomic-level structure and structure-property relationship in metallic glasses, Prog. Mater. Sci. 56 (4) (2011) 379–473.
- [26] Y.Q. Cheng, J. Ding, E. Ma, Local topology vs. atomic-level stresses as a measure of disorder: correlating structural indicators for metallic glasses, Mater. Res. Lett. 1 (1) (2012) 3–12.
- [27] Z. Fan, J. Ding, E. Ma, Machine learning bridges local static structure with multiple properties in metallic glasses, Mater. Today 40 (2020) 48–62.
- [28] L. Ward, S.C. O'Keeffe, J. Stevick, G.R. Jelbert, M. Aykol, C. Wolverton, A machine learning approach for engineering bulk metallic glass alloys, Acta Mater. 159 (2018) 102–111.
- [29] J. Xiong, T.Y. Zhang, S.Q. Shi, Machine learning prediction of elastic properties and glass-forming ability of bulk metallic glasses, MRS Commun. 9 (2) (2019) 576–585.
- [30] S.S. Schoenholz, E.D. Cubuk, D.M. Sussman, E. Kaxiras, A.J. Liu, A structural approach to relaxation in glassy liquids, Nat. Phys. 12 (5) (2016) 469–471.
- [31] E.D. Cubuk, S.S. Schoenholz, J.M. Rieser, B.D. Malone, J. Rottler, D.J. Durian, E. Kaxiras, A.J. Liu, Identifying structural flow defects in disordered solids using machine-learning methods, Phys. Rev. Lett. 114 (10) (2015), 108001.
- [32] C.M. Andolina, P. Williamson, W.A. Saidi, Optimization and validation of a deep learning CuZr atomistic potential: robust applications for crystalline and amorphous phases with near-DFT accuracy, J. Chem. Phys. 152 (15) (2020), 154701.
- [33] J. Helfferich, I. Lyubimov, D. Reid, J.J. de Pablo, Inherent structure energy is a good indicator of molecular mobility in glasses, Soft Matter 12 (27) (2016) 5898–5904.
- [34] D.R. Reid, I. Lyubimov, M.D. Ediger, J.J. de Pablo, Age and structure of a model vapour-deposited glass, Nat. Commun. 7 (1) (2016) 13062.
- [35] Y. Fan, T. Iwashita, T. Egami, Energy landscape-driven non-equilibrium evolution of inherent structure in disordered material, Nat. Commun. 8 (2017) 15417.
- [36] C. Liu, P. Guan, Y. Fan, Correlating defects density in metallic glasses with the distribution of inherent structures in potential energy landscape, Acta Mater. 161 (2018) 295–301.
- [37] Y. Wang, Y. Fan, Incident velocity induced nonmonotonic aging of vapor-deposited polymer glasses, J. Phys. Chem. B 124 (27) (2020) 5740–5745.
- [38] S. Zhang, C. Liu, Y. Fan, Y. Yang, P. Guan, Soft-mode parameter as an indicator for the activation energy spectra in metallic glass, J. Phys. Chem. Lett. 11 (7) (2020) 2781–2787.

- [39] C. Liu, Y. Fan, Emergent fractal energy landscape as the origin of stress-accelerated dynamics in amorphous solids, Phys. Rev. Lett. 127 (21) (2021), 215502.
- [40] Y. Cheng, H. Sheng, E. Ma, Relationship between structure, dynamics, and mechanical properties in metallic glass-forming alloys, Phys. Rev. B 78 (1) (2008), 014207
- [41] F. Zhang, M.I. Mendelev, Y. Zhang, C.Z. Wang, M.J. Kramer, K.M. Ho, Effects of sub-Tg annealing on Cu64.5Zr35.5 glasses: a molecular dynamics study, Appl. Phys. Lett. 104 (6) (2014), 061905.
- [42] D. Şopu, X. Yuan, J. Eckert, Annealing metallic glasses above Tg in order to accelerate the relaxation process in molecular dynamics simulations, Appl. Phys. Lett. 120 (1) (2022), 011904.
- [43] X. Yuan, D. Şopu, F. Moitzi, K. Song, J. Eckert, Intrinsic and extrinsic effects on the brittle-to-ductile transition in metallic glasses, J. Appl. Phys. 128 (12) (2020), 125102
- [44] A. Ninarello, L. Berthier, D. Coslovich, Models and algorithms for the next generation of glass transition studies, Phys. Rev. X 7 (2) (2017), 021039.
- [45] A.P. Bartók, R. Kondor, G. Csányi, On representing chemical environments, Phys. Rev. B 87 (18) (2013), 184115.
- [46] M.O.J. Jäger, E.V. Morooka, F. Federici Canova, L. Himanen, A.S. Foster, Machine learning hydrogen adsorption on nanoclusters through structural descriptors, npj Comput. Mater. 4 (1) (2018) 37.
- [47] C.W. Rosenbrock, E.R. Homer, G. Csányi, G.L.W. Hart, Discovering the building blocks of atomic systems using machine learning: application to grain boundaries, npi Comput. Mater. 3 (1) (2017) 29.
- [48] A.R. Ferreira, Chemical bonding in metallic glasses from machine learning and crystal orbital Hamilton population, Phys. Rev. Mater. 4 (11) (2020), 113603.
- [49] Q. Wang, J. Ding, L. Zhang, E. Podryabinkin, A. Shapeev, E. Ma, Predicting the propensity for thermally activated β events in metallic glasses via interpretable machine learning, npj Comput. Mater. 6 (1) (2020) 194.
- [50] E.R. Homer, High-throughput simulations for insight into grain boundary structure-property relationships and other complex microstructural phenomena, Comput. Mater. Sci. 161 (2019) 244–254.
- [51] X. Liu, X. Li, Q. He, D. Liang, Z. Zhou, J. Ma, Y. Yang, J. Shen, Machine learning-based glass formation prediction in multicomponent alloys, Acta Mater. 201 (2020) 182–190
- [52] Y. Wu, W.H. Wang, P. Guan, H. Bai, Identifying packing features of atoms with distinct dynamic behaviors in metallic glass by machine-learning method, Sci. China Mater. 64 (7) (2021) 1820–1826.
- [53] S. Patala, Understanding grain boundaries the role of crystallography, structural descriptors and machine learning, Comput. Mater. Sci. 162 (2019) 281–294.
- [54] K. Xie, C. Qiao, H. Shen, R. Yang, M. Xu, C. Zhang, Y. Zheng, R. Zhang, L. Chen, K. M. Ho, Neural network potential for Zr–Rh system by machine learning, J. Phys. Condens. Matter 34 (7) (2021), 075402.
- [55] A. Dasgupta, S.R. Broderick, C. Mack, B.U. Kota, R. Subramanian, S. Setlur, V. Govindaraju, K. Rajan, Probabilistic assessment of glass forming ability rules for metallic glasses aided by automated analysis of phase diagrams, Sci. Rep. 9 (1) (2019) 357.

- [56] T. Chen, C. Guestrin, XGBoost: a scalable tree boosting system, in: Proceedings of the 22nd ACM SIGKDD International Conference on Knowledge Discovery and Data Mining, San Francisco, California, USA, Association for Computing Machinery, 2016, pp. 785–794.
- [57] S.M. Lundberg, G. Erion, H. Chen, A. DeGrave, J.M. Prutkin, B. Nair, R. Katz, J. Himmelfarb, N. Bansal, S.I. Lee, From local explanations to global understanding with explainable AI for trees, Nat. Mach. Intell. 2 (1) (2020) 56–67.
- [58] S.M. Lundberg, S.I. Lee, A unified approach to interpreting model predictions, in: I. Guyon, U.V. Luxburg, S. Bengio, H. Wallach, R. Fergus, S. Vishwanathan, R. Garnett (Eds.), Advances in Neural Information Processing Systems, Curran Associates, Inc., 2017.
- [59] B. Wang, L. Luo, E. Guo, Y. Su, M. Wang, R.O. Ritchie, F. Dong, L. Wang, J. Guo, H. Fu, Nanometer-scale gradient atomic packing structure surrounding soft spots in metallic glasses, npj Comput. Mater. 4 (1) (2018) 41.
- [60] P. Zhao, J. Li, J. Hwang, Y. Wang, Influence of nanoscale structural heterogeneity on shear banding in metallic glasses, Acta Mater. 134 (2017) 104–115.
- [61] K. Nomoto, A.V. Ceguerra, C. Gammer, B. Li, H. Bilal, A. Hohenwarter, B. Gludovatz, J. Eckert, S.P. Ringer, J.J. Kruzic, Medium-range order dictates local hardness in bulk metallic glasses, Mater. Today 44 (2021) 48–57.
- [62] S. Im, Y. Wang, P. Zhao, G.H. Yoo, Z. Chen, G. Calderon, M. Abbasi Gharacheh, M. Zhu, O. Licata, B. Mazumder, D.A. Muller, E.S. Park, Y. Wang, J. Hwang, Medium-range ordering, structural heterogeneity, and their influence on properties of Zr-Cu-Co-Al metallic glasses, Phys. Rev. Mater. 5 (11) (2021), 115604.
- [63] S. Im, Z. Chen, J.M. Johnson, P. Zhao, G.H. Yoo, E.S. Park, Y. Wang, D.A. Muller, J. Hwang, Direct determination of structural heterogeneity in metallic glasses using four-dimensional scanning transmission electron microscopy, Ultramicroscopy 195 (2018) 189–193.
- [64] Y. Fan, T. Iwashita, T. Egami, Evolution of elastic heterogeneity during aging in metallic glasses, Phys. Rev. E 89 (06) (2014), 062313.
- [65] J.C. Qiao, Q. Wang, J.M. Pelletier, H. Kato, R. Casalini, D. Crespo, E. Pineda, Y. Yao, Y. Yang, Structural heterogeneities and mechanical behavior of amorphous alloys, Prog. Mater. Sci. 104 (2019) 250–329.
- [66] Y. Sun, A. Concustell, A.L. Greer, Thermomechanical processing of metallic glasses: extending the range of the glassy state, Nat. Rev. Mater. 1 (9) (2016) 1–14.
- [67] C. Zheng, K. Mathew, C. Chen, Y. Chen, H. Tang, A. Dozier, J.J. Kas, F.D. Vila, J. J. Rehr, L.F. Piper, Automated generation and ensemble-learned matching of X-ray absorption spectra, npj Comput. Mater. 4 (1) (2018) 12.
- [68] J. Behler, M. Parrinello, Generalized neural-network representation of highdimensional potential-energy surfaces, Phys. Rev. Lett. 98 (14) (2007), 146401.
- [69] H. Gao, Y. Huang, Geometrically necessary dislocation and size-dependent plasticity. Scr. Mater. 48 (2) (2003) 113–118.
- [70] L. Tian, Y. Fan, L. Li, N. Mousseau, Identifying flow defects in amorphous alloys using machine learning outlier detection methods, Scr. Mater. 186 (2020) 185, 180
- [71] Y. Wang, B. Ghaffari, C. Taylor, S. Lekakh, M. Li, Y. Fan, Predicting the energetics and kinetics of Cr atoms in Fe-Ni-Cr alloys via physics-based machine learning, Scr. Mater. 205 (2021), 114177.